coatings

MDPI

Article

Effects of Ti/Nb Dual-Element Addition on the Microstructure and Properties of Tungsten Carbide-Reinforced Laser Cladding Coatings

Jianfeng Li [1,2,*], Xue Gao [1], Kewei Dong [3] and Jinfu Liu [1]

[1] School of Intelligent Control, Changzhou Vocational Institute of Industry Technology, Changzhou 213164, China; 13585317253@163.com (X.G.); liujinfu@mail.ustc.edu.cn (J.L.)
[2] School of Mechanical and Electrical Engineering, China University of Mining and Technology, Xuzhou 221116, China
[3] School of Materials Science and Engineering, Nanjing University of Science and Technology, Nanjing 210094, China; dongkewei@njust.edu.cn
* Correspondence: ljfcumt@126.com

Abstract: Metal-ceramic composite coatings are produced on the surface of equipment components by laser cladding, improving the abrasive wear resistance of components and extending their service life. However, defects such as brittleness and cracks limit the wide application of metal-ceramic clad coatings in the field of construction machinery. In the present study, a dual-element (Ti/Nb) alloying method is innovatively adopted to regulate the microstructure and mechanical properties of tungsten carbide (WC)-reinforced clad coatings. Experimental results show that with the introduction of Ti/Nb, novel reinforcements are in-situ synthesized in the cladding coatings with two different kinds of morphologies: one is a core-shell carbide with the core of pure TiC and a shell of (Ti,Nb,W)C multiple carbide; the other is a (Ti,Nb,W)C multiple carbide. With 8 wt.% Ti/Nb addition, the newly formed multiple carbides with the appropriate content are well-dispersed and distributed in the clad coating, which effectively transfers load, inhibits the initiation and expansion of micro-cracks, and resists the wear damage of hard abrasive particles, solving the technical problems of the simultaneous improvement of toughness and abrasive wear resistance of metal-ceramic laser cladding coatings.

Keywords: metal-ceramic composite coatings; abrasive wear resistance; dual-element (Ti/Nb) alloying method; multiple carbides

check for updates

Citation: Li, J.; Gao, X.; Dong, K.; Liu, J. Effects of Ti/Nb Dual-Element Addition on the Microstructure and Properties of Tungsten Carbide-Reinforced Laser Cladding Coatings. *Coatings* **2024**, *14*, 708. https://doi.org/10.3390/coatings14060708

Academic Editor: Rafael Comesaña

Received: 26 April 2024
Revised: 17 May 2024
Accepted: 21 May 2024
Published: 4 June 2024

Correction Statement: This article has been republished with a minor change. The change does not affect the scientific content of the article and further details are available within the backmatter of the website version of this article.

Copyright: © 2024 by the authors. Licensee MDPI, Basel, Switzerland. This article is an open access article distributed under the terms and conditions of the Creative Commons Attribution (CC BY) license (https://creativecommons.org/licenses/by/4.0/).

1. Introduction

Laser cladding technology is a method where a high-energy laser beam is employed to irradiate powder materials that are delivered to the surface of metal components, simultaneously melting the powders and a thin layer of the metal substrate surface, and a coating with excellent mechanical and chemical properties is formed on the metal substrate's surface after solidification [1]. Compared with traditional surface technologies, such as brush plating, overlay welding, thermal spray welding, etc., laser cladding is commonly applied for the surface modification of metal components due to its advantages, such as energy concentration, small heat-affected zone, low dilution rate, fine microstructure, superior properties, high degree of automation, and environmental friendliness [2,3].

Tungsten carbide (WC)-reinforced laser cladding coatings organically combine the excellent characteristics of the strength, toughness, and good workability of metal and the high hardness, wear resistance, corrosion resistance, and high-temperature resistance of WC particles [4], making the modified metal components possess outstanding mechanical properties [5]. Ma et al. [6] studied a WC-reinforced Ni-based clad coating on the surface of Q550 steel substrate, and their results showed that the addition of WC reduced the grain size of dendritic crystals, leading to a significant improvement in the clad coating's

microhardness and wear resistance. Tang et al. [7] conducted an investigation that examined the effect of WC nanoparticles addition on the microstructure and mechanical properties of a Ni-based spray welding coating, in comparison to traditional large-sized WC particles. It was concluded that the WC nanoparticles were more evenly distributed in the clad coating and refined its microstructure, which resulted in higher microhardness and lower wear mass loss than when large-sized WC particles are used to reinforce clad coatings. Shu et al. [8] prepared an in-situ WC/Ni-based clad coating by using laser cladding, and the clad coating exhibited excellent mechanical properties due to tight interface bonding between in-situ synthesized WC particles and the coating matrix. However, there remain some defects in WC-reinforced laser-clad coatings, seriously affecting their application in the field of engineering. Firstly, WC has a relatively low free formation enthalpy (38.5 KJ/mol), making it susceptible to dissolution in a high-temperature melt pool, releasing free W and C elements. With the solidification of the melt pool, the $M_{23}C_6$ brittle phases are precipitated due to the metallurgical chemical reactions between W, C, and the alloy elements in the melt pool, which is an important reason why cracks appear in the clad coatings [9,10]. Secondly, WC particles tend to sink in the molten pool due to their higher density (15.7 g cm^{-3}) than those of Fe, Co, and Ni, resulting in a gradient distribution of the highest WC content at the bottom, followed by the middle, and the lowest at the top in the clad coating; hence, uneven mechanical properties in the clad coatings along the depth direction are obtained [11,12]. In order to solve the defects of the WC-reinforced laser-clad coatings, various modification methods are adopted by scholars both domestically and internationally. The adjustment of process parameters is primarily considered. Zhao et al. [13] reported the effects of process parameters on the microstructure of WC/Ni60 clad coatings. Their results indicated that defects such as pores and cracks did not appear in the clad coatings, and the microstructure was well-homogenized. However, the effects of regulating metal-ceramic clad coatings through the optimization of process parameters are limited. External energy field-assisted laser cladding processes, such as ultrasonic vibration and electromagnetic assistance, etc., are methods that have been considered secondarily. Huo et al. [14] fabricated IN718/WC composite coatings using an electromagnetic compound field-assisted laser cladding method. The composite electromagnetic field generated a downward Ampere force that intensified the Marangoni flow within the molten pool, prompting WC particles to be evenly distributed in the clad coating, thereby improving the mechanical properties of the clad coating. However, the structure and size of metal components are strictly required using the electromagnetic assistance preparation method, limiting its universal applicability. The alloying method is also often used. Ma et al. [15] studied the modification of Ti element on the microstructure and properties of Ni60/WC clad coatings. It was found that the addition of Ti promoted the dissolution of primary WC particles, leading to the formation of new TiC, and inhibited the generation of brittle phase $M_{23}C_6$. Compared to the Ni60/WC clad coatings, the Ti-Ni60/WC clad coating not only had a uniform microstructure, but also demonstrated superior wear resistance. Based on the above three modification methods, the alloying method is more suitable for solving the defects of WC-reinforced laser-clad coatings given its advantages of simple operation, good regulatory effect, and no requirements for the structure and size of metal components. According to some previous studies [16,17], multiple alloying elements had the better modification effect on the laser cladding coatings than single elements. However, so far, the researches on the modification of WC-reinforced clad coatings using alloying have mainly focused on single alloying elements, while few studies of modification with multiple alloying elements have been reported.

Therefore, in this paper, Fe60 self-fluxing alloy, WC, Ti, and Nb powders are used as raw materials to prepare Ti/Nb-modified WC/Fe clad coatings using laser cladding technology. The effects of the different Ti/Nb content added on the microstructure, crack sensitivity, and the abrasive wear resistance of the WC/Fe clad coatings are systematically studied. The experimental results in this study are helpful to solve the technical problem of simultaneously improving the wear resistance and crack resistance of WC/Fe clad coatings,

having significant application value for the surface modification of metal components serving in a dual impact-wear environment.

2. Experimental Procedure

16Mn steels were used as the substrate. The surfaces of the steel were polished, then washed before the experiments. Commercial Fe60 self-fluxing alloy, WC, Ti, and Nb powders were selected to be cladding materials, and all the powders were spherical. Fe60 self-fluxing alloy powder with a particle size of 40 μm~120 μm was employed to be the matrix of the clad coatings. The WC, Ti, and Nb powders were adopted as additives, with particle sizes ranging from 15 μm to 40 μm, 10 μm to 50 μm, and 2 μm to 20 μm, respectively. The nominal chemical compositions of the substrate in wt.% were 1.2~1.6 Mn, 0.2~0.6 Si, 0.1~0.2 C, ≤0.3 Cr, ≤0.03 S, ≤0.03 P, ≤0.25 Cu, and bal. Fe. The chemical compositions of the Fe60 self-fluxing alloy powder in wt.% were 0.1~1.0 Ni, 13~17 Cr, 0.5~1.0 C, 0.3~1.0 Si, 0.2~1.5 B, and bal. Fe.

Table 1 gives the compositions of the designed cladding materials. The Fe60 self-fluxing alloy, WC, Ti and Nb powders were well-mixed in a vacuum planetary ball mill for cladding materials. Afterwards, well-mixed cladding materials were dried in a vacuum drying oven for sufficient time to remove any water.

Table 1. Chemical compositions of cladding materials (in wt.%).

No.	Fe60	WC	Ti	Nb
1	78	20	0.68	1.32
2	76	20	1.36	2.64
3	72	20	2.72	5.28

An HWL-R1500W laser system was used in the process of laser cladding. High-purity Ar was supplied through the same coaxial nozzle to protect the high-temperature molten pool from oxidation. The processing parameters of the laser cladding were a laser power of 1500 W, a scanning speed of 240 mm min^{-1}, a powder feeding rate of 10 g min^{-1}, and a laser beam diameter of 2 mm in this experiment. The microstructural characterizations of the object were a single-track coating, and multi-track coatings with 50% overlapping ratio were employed for the X-ray diffraction (XRD) and abrasive wear tests.

All the samples were cut along the cross-section, and then sliced samples were further polished according to standard metallographic procedures. For microstructural observations, a Kroll's solution of ethanol and HNO_3 with a volume ratio of 19:1 was applied to etch the specimens. A scanning electron microscope (SEM) and a transmission electron microscope (TEM) were utilized to observe the microstructure, and elemental scanning analysis for phases was conducted via an energy dispersive spectrometer (EDS). Phase constituents were identified by means of X-ray diffraction (XRD).

The microhardness profiles of all single-track coatings, from the surface of the coatings to the coatings/substrate interface, were examined with a Vickers hardness tester (MTHV-1MMDTe) with a 500 g load and a 10 s load-dwell time, and the average values were calculated. For assessment of cracking sensitivity, cracks in specimens with the sizes of 60 mm × 30 mm × 10 mm were measured with the coloration method. The abrasive wear resistance of all the specimens was evaluated with a self-designed abrasive wear tester; the device and its structural diagram are shown in Figure 1. Measuring parameters of the abrasive wear tests included a load of 200 N, a diameter/thickness of wheel of 178/30 mm, a rotating speed of 200 r/min, a testing time of 60 min, and a wear medium of coal gangue, respectively. To ensure reliable data, the experiment was conducted identically three times. The abrasive wear resistance of the specimens was characterized in terms of their mass loss, and the wear mass loss of all the specimens was measured by an electronic balance with an accuracy of ±0.1 mg after the wear test. The wear mechanism of the specimens was revealed by observing wear scars.

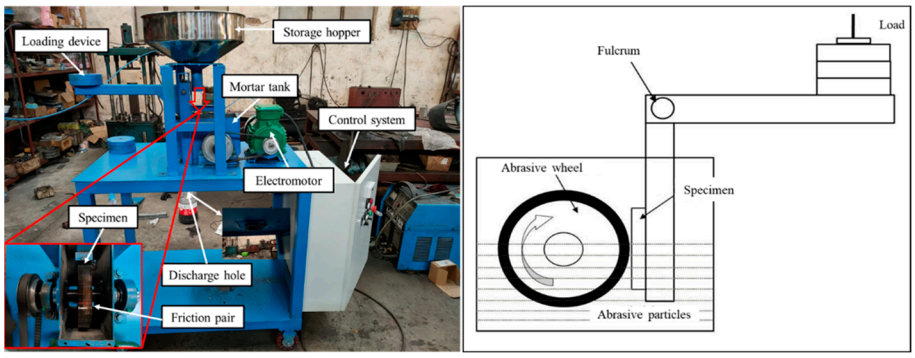

Figure 1. Photograph and structural diagram of the abrasive wear tester.

3. Results and Discussion

3.1. Microstructure Analysis

The microstructures of different Ti/Nb-containing coatings/substrate interfaces are indicated in Figure 2. Clearly, no obvious defects, such as cracking and pores, occur in the clad coatings or at the boundaries of the clad coatings. Moreover, the planar crystal growth between clad coatings and substrates is observed. It suggests that good metallurgical joints between clad coatings and substrates are formed.

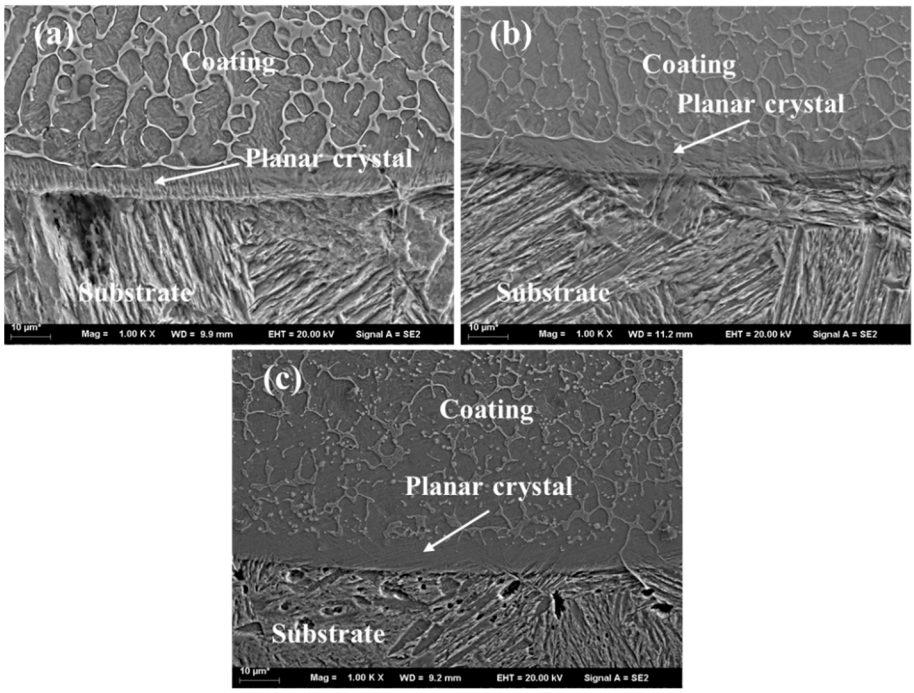

Figure 2. Microstructures of different Ti/Nb-containing coating/substrate interfaces: (**a**) 2%; (**b**) 4%; (**c**) 8%.

The microstructures of the clad coatings with different Ti/Nb content are shown in Figure 3. According to our previous study [9], the clad coating without Ti/Nb was mainly composed of α-Fe supersaturated solid solutions, inter-dendritic $M_{23}C_6$ carbides (M: Cr, W, Fe) and reprecipitated WC particles. With Ti/Nb addition, the content of brittle phase $M_{23}C_6$ in the clad coating is decreased, and few reprecipitated WC particles are found, but reinforcements with two different kinds of morphologies are precipitated in the clad coatings: one is a core-shell structure; the other is a no-cored and homogeneous structure. Obviously, the content of core-shell precipitates is much higher than that of no-cored precipitates. Furthermore, the amount of inter-dendritic $M_{23}C_6$ carbides obviously decreases. The above results suggest that the precipitation of reinforcements reduces the

amount of $M_{23}C_6$ in the clad coating. The decrease in $M_{23}C_6$ leads to a reduction in the brittleness of the grain boundaries, thereby toughening the clad coating. Additionally, the particle size and number of reinforcements are increased as well with an increase in the amount of Ti/Nb added, but always remain in the form of equiaxial granular particles. It is worth noting that the average particle size of the core-shell reinforcements is greatly larger than that of the no-cored reinforcements.

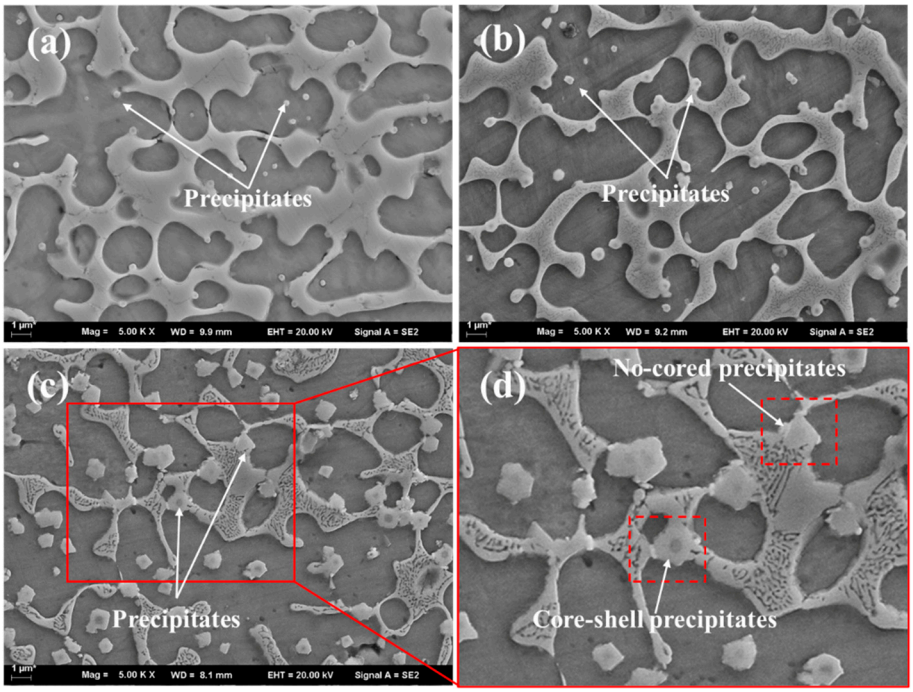

Figure 3. Microstructures of the clad coatings with different Ti/Nb content: (**a**) 2%; (**b**) 4%; (**c**) 8%; (**d**) Enlarged view of red rectangle.

In order to further study the specific distribution of alloy elements in the precipitates with two different kinds of structural morphologies, the elemental distributions of Fe, Cr, Ti, Nb, W, and C elements in the two precipitates are shown in Figures 4 and 5, respectively. Clearly, both precipitates are enriched with C, W, Nb, and Ti elements, but a significant difference in the distribution is observed. Ti, Nb, W, and C elements are evenly distributed in the no-cored precipitates, but in the core-shell precipitates, there is an obvious concentration gradient in the distribution of Ti, Nb, W, and C elements. Only Ti and C elements are detected in the core without other alloy elements; Ti, Nb, W, and C elements are concentrated in the shell. It is worth noting that the concentration of Ti and C elements in the core is much higher than in the shell. Considering the results shown in Figure 4, it is further inferred that the core-shell precipitates consist of the core of pure TiC carbides and the shell of the (Ti,Nb,W)C multiple carbides, and the no-cored precipitates are the (Ti,Nb,W)C multiple carbides.

Because the two precipitates underwent the same melting process, the reason for the formation of two different kinds of morphologies is mainly attributed to different chemical compositions. Based on our previous studies, TiC and NbC were dissolved mutually to form (Ti,Nb)C multiple carbides due to the satisfaction of the Hume–Rothery condition. Similarly, the difference in the atomic radius between Ti and W is 0.004 nm, and the difference in the atomic radius between Nb and W is 0.007 nm. Thus, the differences in the atomic radius between Ti and W, Nb and W are 2.7% and 4.7%, respectively, which are much less than 15%. It means that TiC, WC, and NbC are also dissolved mutually to form (Ti,Nb,W)C multiple carbides due to the satisfaction of the Hume–Rothery condition. Besides, with 8% Ti/Nb addition, white and irregular-shaped precipitates are formed and attach to the surface of the core-shell and no-cored precipitates for nucleation growth.

According to the analysis results in Figure 5, the white and irregular-shaped precipitates are mainly rich in the W element, and there exists also the enrichment of Cr elements. It can be concluded that the white and irregular-shaped precipitates should be the W-rich compounds with a solid solution of Cr elements. The solid solution of Cr elements in the W-rich compounds is possibly caused by the rapid solidification process of the laser melt pool.

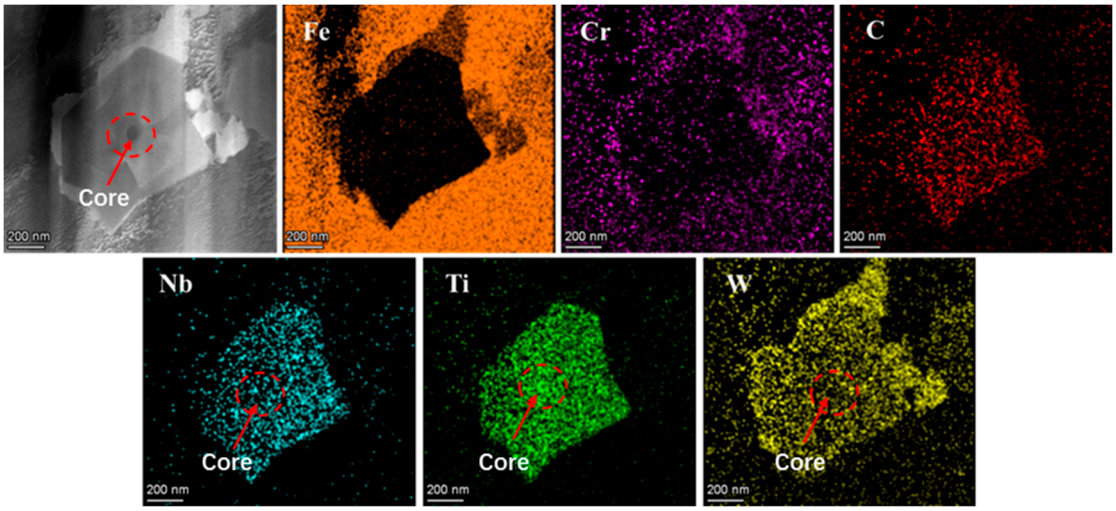

Figure 4. Mapping analysis of Fe, Cr, Ti, Nb, W, and C elements in the core-shell precipitates.

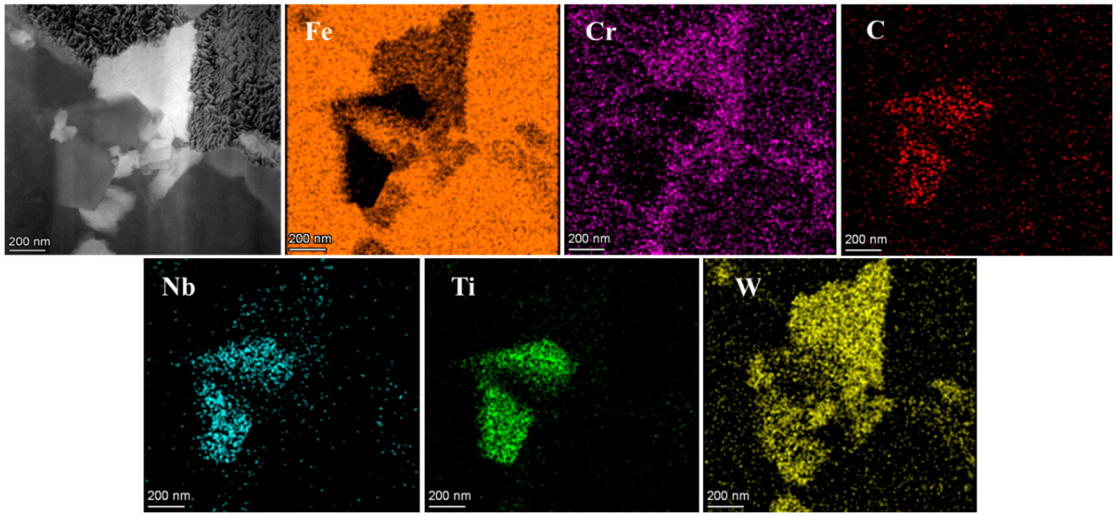

Figure 5. Mapping analysis of Fe, Cr, Ti, Nb, W, and C elements in the no-cored precipitates.

The SAED patterns of the core-shell and no-cored precipitates are further conducted by TEM, as shown in Figure 6. As seen, the binding interfaces between the two precipitates and the Fe matrix are straight, purity-free, and enriched with none of the elements, which is well consistent with the excellent characteristics of in-situ synthesized reinforcements. The in-situ synthesis of reinforcements was firmly bound to the Fe matrix, which is beneficial to improving the mechanical properties of the clad coatings [18]. Furthermore, there are obvious grain boundaries at the shell of the core-shell reinforcements, indicating that the shell of the core-shell reinforcements is composed of multiple (Ti,Nb,W)C particles rather than a single (Ti,Nb,W)C particle. Last but not least, the core-shell and no-cored reinforcements share the same crystal zone axis [001] as TiC and NbC, further indicating that the two reinforcements have the same crystal structure and orientation as TiC and NbC. As such, the above inference that the core-shell precipitates are composed of a core of pure

TiC carbides and a shell of (Ti,Nb,W)C multiple carbides, and the no-cored precipitates are composed of (Ti,Nb,W)C multiple carbides, is further verified.

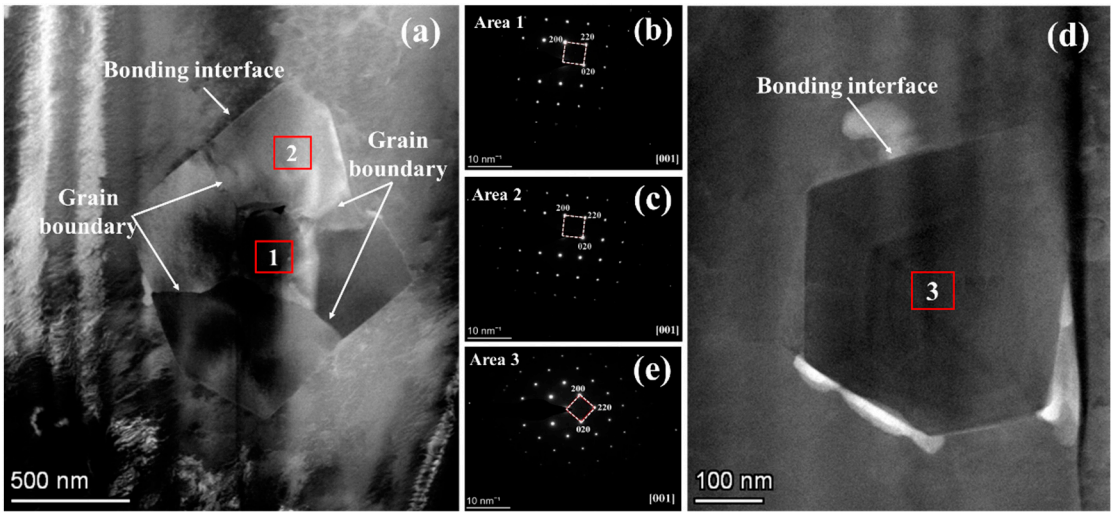

Figure 6. TEM image and the corresponding SEAD pattern: (**a**) TEM image of the core-shell precipitates; (**b**) SEAD pattern of core of the core-shell precipitates; (**c**) SEAD pattern of shell of the core-shell precipitates (**d**) TEM image of the no-cored precipitates; (**e**) SEAD pattern of the no-cored precipitates.

Figure 7 shows the particle size and distribution density of multiple carbide particles in the clad coatings with different Ti/Nb content. It can be seen that the particle size and distribution density of multiple carbide particles show a linear increasing trend with the increase of Ti/Nb. It is because as the amount of Ti/Nb added increases, the concentration of Ti and Nb elements in the melt pool increases, and in turn increases the concentration of Ti and Nb in the vicinity of C atoms, which ultimately enhances the nucleation and growth of multiple carbides, resulting in an increase in both the particle size and distribution density of multiple carbide particles at the same time. As the distribution density and particle size of composite carbides in the clad coatings increase, the mechanical properties of the composite carbides-reinforced clad coatings are further improved, which is mainly due to the enhancement of the dispersion strengthening effect of the composite carbide particles.

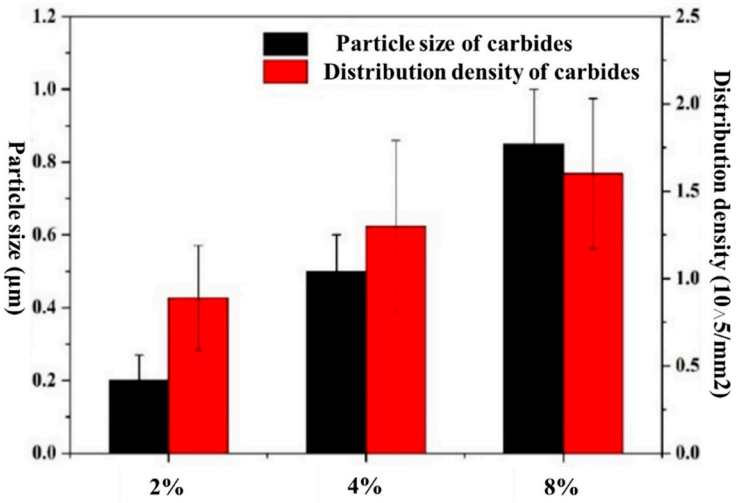

Figure 7. Density and size of multiple carbide particles in the clad coatings with different Ti/Nb content.

The distribution characteristics of multiple carbide particles in the coatings with the addition of 4% and 8% Ti/Nb are shown in Figure 8. Obviously, the multiple carbide

particles are evenly distributed at the bottom, middle, and top of the clad coatings. There is no gradient distribution trend like that seen in WC and other high-density carbide particles, where the content is highest at the top, followed by the middle, and lowest at the top. Neither is there a trend similar to TiC and other low-density carbide particles, which shows low content at the bottom, followed by the middle, and highest at the top.

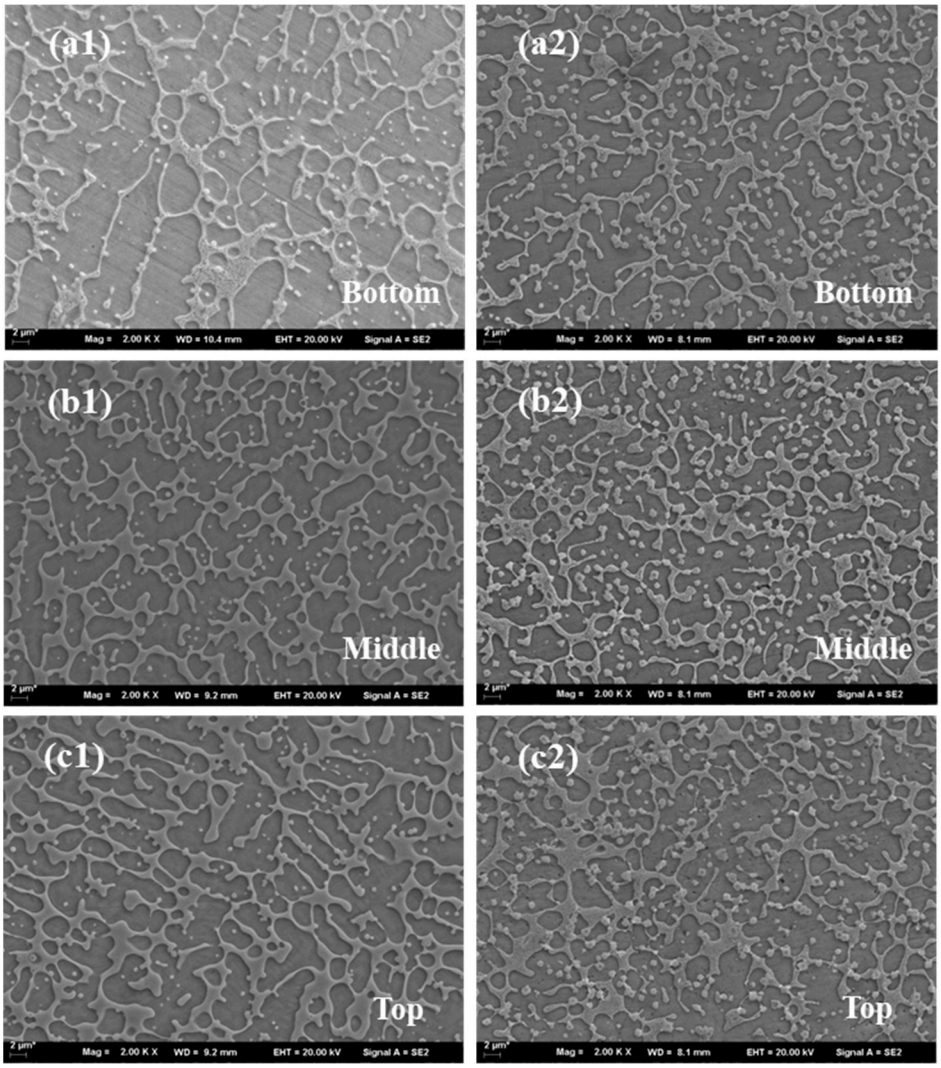

Figure 8. Distribution of multiple carbide particles in the clad coatings with different Ti/Nb content: (**a1**–**c1**) 4%; (**a2**–**c2**) 8%.

According to the above analysis, the multiple carbide particles are formed by the mutual diffusion and solid solution of WC, TiC, and NbC at high temperatures. NbC has a density similar to Fe (ρ_{NbC}: 7.78 g cm^{-3}, ρ_{Fe}: 7.87 g cm^{-3}), the density of TiC (ρ_{TiC}:4.93 g cm^{-3}) is much lower than that of Fe, and the density of WC (ρ_{WC}: 15.7 g cm^{-3}) is much higher than that of Fe. Therefore, as the solid solution is formed by the mutual solid solution of WC, TiC, and NbC, the comprehensive density of multiple carbide particles is close to that of the Fe matrix alloy, which is also the reason why the multiple carbide particles are evenly distributed in the clad coatings and do not show a gradient distribution trend at the bottom, middle, and top of the clad coating. Similar results were also reported in the study of Ashok Kumar Srivastava et al. [19]. The uniform distribution of multiple carbide particles ensures the even microstructure of the clad coatings, and then makes the mechanical properties of the clad coatings uniform along the depth direction. In addition, as shown in Figure 8, it can also be observed that most of the precipitated multiple carbide particles are embedded within the dendritic regions of the clad coatings, while only a

small portion is located in the inter-dendritic regions. The reason can be explained as follows. A study pointed out [20] that during the cooling crystallization process of metal in a high-temperature molten pool, there was a critical velocity of "capture" associated with the forward movement of the solid-liquid interface. The critical velocity of "capture" was closely related to the ratio of the thermal conductivity between the metal alloy and precipitated particles [21]. If the critical velocity of "capture" was greater than the advanced velocity of the solid-liquid interface, the precipitated particles would be pushed forward to the unsolidified region together, and finally precipitated particles would be embedded in the inter-dendritic regions of the clad coatings. Similarly, if the critical velocity of "capture" was less than the advanced velocity of the solid-liquid interface, the precipitated particles could be captured by the solid-liquid interface, and eventually the precipitated particles would be embedded in the dendritic regions of the clad coatings. The thermal conductivity coefficient of the metallic liquid phase and the precipitated phase was set as $\alpha = k_{particle}/k_{metal\ matrix}$, which had a great influence on the solidification around the precipitated particles. If $\alpha > 1$, the solid–liquid interface would sink down, and the metal liquid phase would have a great phagocytic force on the precipitated particles, making the precipitated particles become "trapped"; if $\alpha \leq 1$, the solid-liquid interface would have a strong repulsive force on the precipitated particles. It is well known that the thermal conductivity of the Fe matrix is 80 W/m·K, and the thermal conductivities of TiC, NbC, and WC particles are 21.0 W/m·K, 14.0 W/m·K, and 121.0 W/m·K, respectively. Therefore, the thermal conductivity of precipitated multiple carbide particles in this study is as follows: 14.0 W/m·K < $k_{multiple\ carbide\ particles}$ < 121.0 W/m·K. Combined with the distribution characteristics of multiple carbide particles in the clad coatings, it can be further concluded that the precipitated multiple carbide particles are "trapped" by the solid–liquid interface ($\alpha > 1$). The multiple carbide particles are uniformly distributed in the Fe matrix, forming a typical intracrystalline composite structure, playing a more significant role in strengthening the clad coatings.

3.2. Mechanical Properties

Figure 9 shows the microhardness values of the clad coatings with different Ti/Nb from the surface of the coatings to the coatings/substrate interface. As observed, the microhardness distribution of the clad coatings are stable from the surface of coating to the coating/substrate interface after the introduction of Ti/Nb. This stability is most pronounced with the Ti/Nb content increasing to 8%. At this level, the microhardness remains consistent from the top to the bottom of the clad coating, indicating that the clad coating shows a uniform microstructure and mechanical properties. This further confirms that the multiple carbide particles are evenly dispersed throughout the clad coatings. Furthermore, with an increase of Ti/Nb from 2% to 8%, the microhardness of the clad coatings is decreased linearly. As the content of Ti/Nb added reaches 8%, the average microhardness value of the clad coatings is the lowest, only about $410HV_{0.5}$, which is reduced by over 50% compared with the Ti/Nb-free coating (about $931.4HV_{0.5}$; the result was shown in a previous study [9]). Based on the above microstructure analysis, it can be seen that the main reason for the decrease in microhardness of the Ti/Nb-containing coating is the introduction of strong carbide-forming elements Ti and Nb. C elements in the high-temperature molten pool are consumed by Ti and Nb elements, not only reducing the solid solution of C elements in the coatings' matrix, but reducing the precipitation of brittle phase $M_{23}C_6$ carbides in the inter-dendritic regions. The precipitation of multiple carbide particles reduces the C content in the matrix of the clad coatings, not only strengthening the toughness of the clad coatings, but also improving the abrasive wear resistance.

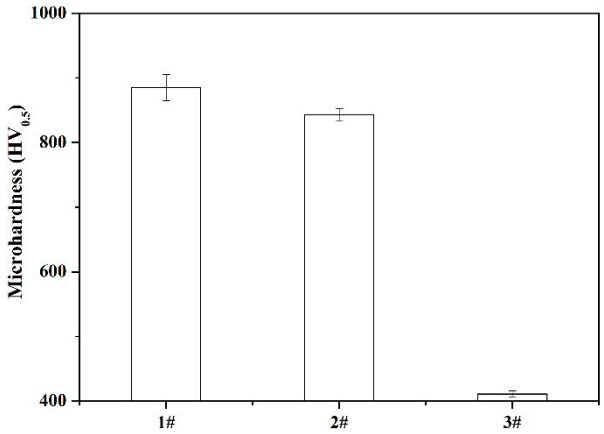

Figure 9. Microhardness value of the clad coatings with different Ti/Nb from the surface of coatings to the coatings/substrate interface.

Table 2 lists the crack detection data of the clad coatings with different Ti/Nb. When the addition of Ti/Nb is 2%, over eight cracks are generated in the clad coating, indicating that the 2% Ti/Nb-containing coating has a relatively high crack sensitivity. It is because the dissolution of WC releases a large number of W and C elements into the high-temperature melt pool, and a large amount of the brittle phase $M_{23}C_6$ carbides are formed by the chemical reactions between W and C elements and alloying elements such as Cr, Fe, etc., thus increasing the crack sensitivity of the clad coating. As the content of Ti/Nb further increased, the number of cracks in the clad coatings decreases, especially as the Ti/Nb content reaches 8%, at which point the clad coating is dense and crack-free. This indicates that the 8% Ti/Nb-containing coating has the lowest crack sensitivity and excellent toughness. It is widely believed that the microhardness and the toughness of materials are negatively correlated. Thus, the above result of the 8% Ti/Nb-containing coating with the lowest microhardness once again proves that the 8% Ti/Nb-contained coating has the most outstanding toughness among all the coatings.

Table 2. Non-destructive test results of the clad coatings with different Ti/Nb.

No.	Number of Cracks
1#	$n > 8$
2#	$1 \leq n < 4$
3#	0

The reasons for the decrease in the crack sensitivity of the Ti/Nb-containing coatings are as follows: Firstly, the strong carbide-forming elements Ti and Nb have a greater affinity than Fe, Cr, and other elements, and the introduction of them will preferentially combine with C elements in the molten pool to precipitate carbides such as TiC, NbC, etc., reducing the precipitation amount of intergranular brittle phase $M_{23}C_6$ carbides. The existence of brittle phase $M_{23}C_6$ is an important factor leading to the cracking of the clad coatings [22]. Secondly, the precipitated composite carbide particles are evenly distributed in the clad coatings, which has a great second-phase dispersion strengthening effect than traditional carbide particles, effectively preventing the initiation and propagation of micro-cracks in the clad coatings.

Figure 10 shows the wear mass loss of the clad coatings with different Ti/Nb content after the wear tests. With the amount of Ti/Nb added increasing from 2%→4%→8%, the wear mass loss of the clad coatings after wear testing presents a trend of first increasing and then sharply decreasing. As the amount of Ti/Nb added reaches 8%, the average wear mass loss of the clad coating is only about 22.1 mg, reaching the lowest value among all the Ti/Nb-containing coatings. According to the above analysis results of microhardness and crack

sensitivity of the Ti/Nb-containing coatings, the 8% Ti/Nb-containing coating possesses the lowest microhardness, but excellent toughness and abrasive wear resistance. Generally, materials with low hardness have poor wear resistance. However, despite the very low hardness, the 8% Ti/Nb-containing coating shows outstanding wear resistance, which is mainly attributed to the fact that the wear resistance of the composite materials relates not only to the hardness, but also to the volume fraction, distribution, shape, hardness, particle size, and bonding strength with the material matrix of second-phase hard particles [23]. As such, the large particle size, high distribution density, and uniform dispersion of formed multiple carbide particles are the main reason for the excellent abrasive wear resistance of the 8% Ti/Nb-containing coating.

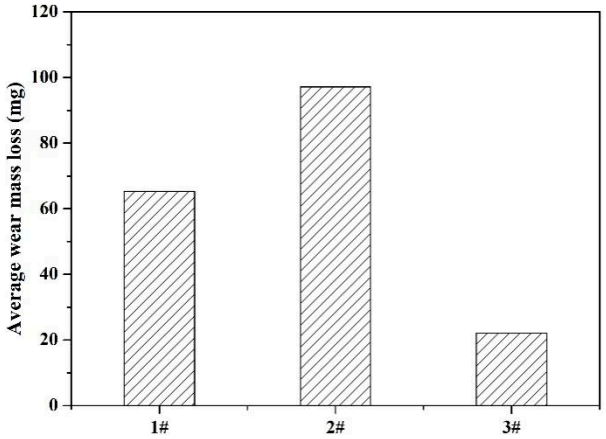

Figure 10. Average wear mass loss of the clad coatings with different Ti/Nb.

The main wear mechanism of the clad coatings with different Ti/Nb content are further explored, and the worn morphologies of the clad coatings are shown in Figure 11. Clearly, with 2% Ti/Nb introduction, wide grooves, serious plastic deformation, and spalling of reinforced particles are detected on the worn surface of the clad coating, the wear mechanism of which is serious abrasive wear, plastic deformation, and particles shedding. Hence, the 2% Ti/Nb-containing coating shows poor abrasive wear resistance due to its relatively low hardness. Similarly, because the 4% Ti/Nb-containing coating has a relatively low hardness and high wear mass loss compared to the 2% Ti/Nb-containing coating, the 4% Ti/Nb-containing coating suffers more serious abrasive wear and plastic deformation than the 2% Ti/Nb-containing coating. However, interestingly, with the addition of Ti/Nb increasing to 8%, few grooves and little plastic deformation are observed on the worn surface of the clad coating with the lowest hardness, and only thin scratches are found. Additionally, the hard reinforcement particles, that is, the newly-generated multiple carbide particles, are densely embedded on the worn surface and remain convex without no sign of falling off, indicating that the 8% Ti/Nb-containing coating has excellent abrasive wear resistance, and its main wear mechanism is slight abrasive wear, consistent with the result of the lowest wear mass loss of the 8% Ti/Nb-containing coating shown in Figure 10.

When the addition of Ti/Nb added is relatively low (2% and 4%), the formed multiple carbide particles are fewer and smaller. At the initial stage of the wear process, the matrix of the clad coatings is primarily worn due to its low hardness. With the wear time progressing, the multiple carbide particles embedded in the clad coatings are gradually exposed on the worn surfaces of the clad coatings. The exposed multiple carbide particles can effectively resist abrasive wear. However, the multiple carbide particles are sparsely distributed, fine, and have a relatively large average spacing between them, which causes them to be unable to protect the Fe matrix from wear damage, allowing the Fe matrix to continue being worn away. With the further wear of the Fe matrix, the bonding areas between the Fe matrix and the multiple carbide particles gradually decrease, resulting in the reduction of the bonding strength between the multiple carbide particles and the Fe matrix. As the Fe matrix is

worn to a certain extent, micro-cracks are formed and expanded at the bonding interface between the Fe matrix and the multiple carbide particles under the cyclic scratching action of abrasive particles, eventually leading to the falling of the carbide particles from the worn surfaces of the clad coatings. The anti-wear action of the composite carbide particles is resisted, increasing the wear mass loss of the clad coatings, which corresponds exactly to the wear mechanism of 2% and 4% Ti/Nb-containing coatings shown in Figure 12a. The multiple carbide particles formed in the 8% Ti/Nb-containing coating show high content, large size, and small spacing between the multiple carbide particles. As the matrix of the clad coating is worn down, the multiple carbide particles become exposed and slightly convex on the worn surface, causing the abrasive particles to be mainly in contact with the carbide particles, effectively protecting the Fe matrix from further wear. Therefore, the wear mass loss of the 8% Ti/Nb-containing coating is reduced, and the anti-wear property of the 8% Ti/Nb-containing coating is improved, corresponding to the wear mechanism shown in Figure 12b.

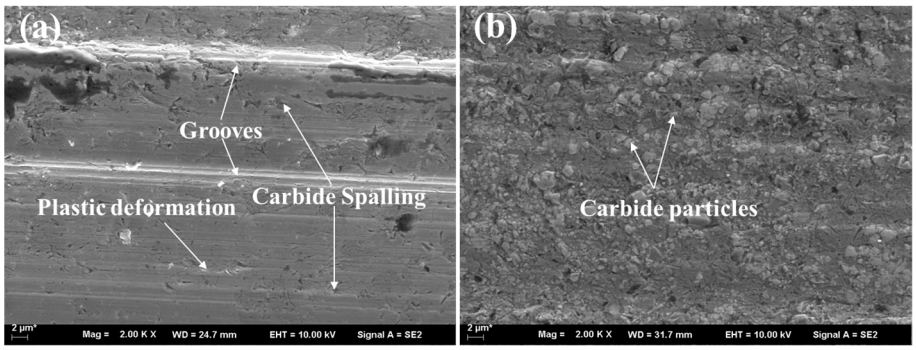

Figure 11. Worn morphologies of clad coatings with different Ti/Nb: (**a**) 2%; (**b**) 8%.

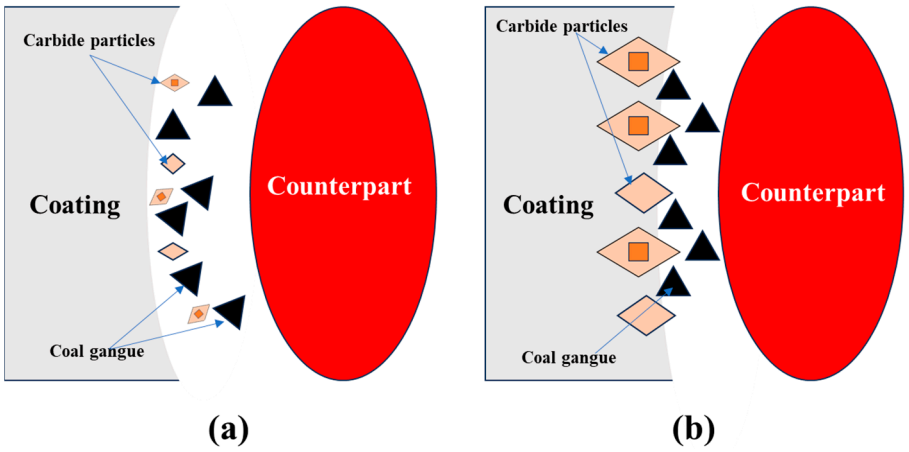

Figure 12. Wear mechanisms of clad coatings with different Ti/Nb:(**a**) 2%, 4%; (**b**) 8%.

4. Conclusions

In the present study, a dual-element (Ti/Nb) alloying method is adopted to regulate the microstructure and mechanical properties of a tungsten carbide (WC)-reinforced clad coating. Based on the above results, the following conclusions are drawn:

1. With the Ti/Nb introduction, novel reinforcements are in-situ synthesized in the clad coatings with two different kinds of morphologies: one is a core-shell carbide with the core of pure TiC and the shell of (Ti,Nb,W)C multiple carbide; the other is a (Ti,Nb,W)C multiple carbide.
2. With 8 wt.% Ti/Nb addition, newly formed multiple carbides with the appropriate content are well-dispersed and distributed in the clad coating, which effectively transfers load, inhibits the initiation and expansion of micro-cracks, and resists the

wear damage of hard abrasive particles, solving the technical problems of the simultaneous improvement of toughness and wear resistance of metal-ceramic laser cladding coatings.

Author Contributions: J.L. (Jianfeng Li) conceived and designed the experiments; J.L. (Jianfeng Li) performed the experiments; J.L. (Jianfeng Li) analyzed the data; X.G., K.D. and J.L. (Jinfu Liu) provided useful comments for this study. All authors have read and agreed to the published version of the manuscript.

Funding: The authors would like to express their gratitude for financial support from the General Project of Natural Science Foundation of Colleges and Universities of Jiangsu Province (23KJB460002), Qinglan Project of Colleges and Universities of Jiangsu Province, the Natural Science Fund of Jiangsu Province (BK20220241), the National Natural Science Foundation of China (52301051), and the Doctoral Fund Project Support of Changzhou Vocational Institute of Industry Technology (BS202313101001).

Institutional Review Board Statement: Not applicable.

Informed Consent Statement: Not applicable.

Data Availability Statement: Data are contained within the article.

Conflicts of Interest: The authors declare no conflict of interest.

References

1. Wu, T.; Shi, W.Q.; Xie, L.Y.; Gong, M.M.; Huang, J.; Xie, Y.P.; He, K.F. Forming quality control method of laser cladding Fe-based TiC composite coating. *Laser Technol.* **2022**, *46*, 344–354. (In Chinese)
2. Yu, J.S.; He, S.X. Research on Fabrication and Properties of Ni-Base Composite Coating by Laser Cladding. *Appl. Laser* **2023**, *43*, 90–96. (In Chinese)
3. Fazlianaa, F.; Aqidaa, S.N.; Ismailc, I. Effect of tungsten carbide partial dissolution on the microstructure evolution of a laser clad surface. *Opt. Laser Technol.* **2020**, *121*, 105789. [CrossRef]
4. Zhang, Y.; Lou, L.Y.; Xu, Q.L.; Li, Y.; Li, C.J.; Li, C.X. Microstructure and Wear Resistance of Ni-Based WC Coating by Ultra-High Speed Laser Cladding. *Acta Metall. Sin.* **2020**, *56*, 1530–1540. (In Chinese)
5. Huebner, J.; Rutkowski, P.; Kata, D. Microstructural and Mechanical Study of Inconel 625—Tungsten Carbide Composite Coatings Obtained by Powder Laser Cladding. *Arch. Metall. Mater.* **2017**, *62*, 531–538. [CrossRef]
6. Ma, Q.S.; Li, Y.J.; Wang, J.; Liu, K. Investigation on cored-eutectic structure in Ni60/WC composite coatings fabricated by wide-band laser cladding. *J. Alloys Compd.* **2015**, *645*, 151–157. [CrossRef]
7. Tang, K.K.; Ding, Z.X.; Li, C. Microstructure and Abrasive Wear Resistance of Nano-WC Reinforced Ni-based Alloy Spray-melted Coatings. *Surf. Technol.* **2017**, *46*, 27–32. (In Chinese)
8. Shu, D.; Li, Z.; Zhang, K.; Yao, C.; Li, D.; Dai, Z. In situ synthesized high volume fraction WC reinforced Ni-based coating by laser cladding. *Mater. Lett.* **2017**, *195*, 178–181. [CrossRef]
9. Li, J.F.; Zhu, Z.C.; Peng, Y.X.; Shen, G. A comparative study on microstructure evolution and wear resistance of different-sized tungsten carbide modified Fe-based laser cladding coatings. *Opt. Laser Technol.* **2022**, *147*, 107672. [CrossRef]
10. Li, J.F.; Zhu, Z.C.; Peng, Y.X.; Shen, G. Phase evolution and wear resistance of in-situ synthesized $(Cr,W)_{23}C_6$-WC composite ceramics reinforced Fe-based composite coatings produced by laser cladding. *Vacuum* **2021**, *190*, 110242. [CrossRef]
11. Wang, K.M.; Du, D.; Liu, G.; Chang, B.H.; Hong, Y.X. Microstructure and properties of WC reinforced Ni-based composite coatings with Y_2O_3 addition on titanium alloy by laser cladding. *Sci. Technol. Weld. Join.* **2019**, *24*, 517–524. [CrossRef]
12. Guo, C.; Zhou, J.S.; Chen, J.M.; Zhao, J.R.; Yu, Y.J.; Zhou, H.D. High temperature wear resistance of laser cladding NiCrBSi and NiCrBSi/WC-Ni composite coatings. *Wear* **2011**, *270*, 492–498. [CrossRef]
13. Zhao, W.; Zhang, K.; Liu, P.; Ma, F.C.; Chen, X.H.; Liu, X.K. Microstructure and Properties of Ni-based WC Composite Cladding Coatings by laser cladding. *Funct. Mater.* **2019**, *50*, 1098–1103. (In Chinese)
14. Huo, K.; Zhou, J.Z.; Dai, F.Z.; Xu, J.L. Particle distribution and microstructure of IN718/WC composite coating fabricated by electromagnetic compound field-assisted laser cladding. *Appl. Surf. Sci.* **2021**, *545*, 149078. [CrossRef]
15. Ma, Q.S.; Li, Y.J.; Wang, J. Effects of Ti addition on microstructure homogenization and wear resistance of wide-band laser clad Ni60/WC composite coatings. *Int. J. Refract. Met. Hard Mater.* **2017**, *64*, 225–233.
16. Li, Q.T.; Lei, Y.P.; Fu, H.G. Growth mechanism, distribution characteristics and reinforcing behavior of (Ti,Nb)C particle in laser cladded Fe-based composite coating. *Appl. Surf. Sci.* **2014**, *316*, 610–616. [CrossRef]
17. Wang, X.H.; Zhang, M.; Du, B.S.; Qu, S.Y.; Zou, Z.D. Microstructure and wear properties of in situ multiple carbides reinforced Fe based surface composite coating produced by laser cladding. *Mater. Sci. Technol.* **2010**, *26*, 935–939. [CrossRef]
18. Du, B.S. Study on In Situ Synthesized Ceramic Phase Reinforced Fe-based Coatings by Laser Cladding. Ph.D. Thesis, Shandong University, Jinan, China, 2009. (In Chinese)

19. Srivastava, A.K.; Das, K. Microstructure and abrasive wear study of (Ti,W)C-reinforced high-manganese austenitic steel matrix composite. *Mater. Lett.* **2008**, *62*, 3947–3950. [CrossRef]
20. Yong, Y.W. Study on Process and Performance of Laser Cladding Nickel Based Composite Coatings. Ph.D. Thesis, Shanghai Jiao Tong University, Shanghai, China, 2018. (In Chinese).
21. Shangguan, D.; Ahuja, S.; Stefanescu, D.M. An analytical model for the interaction between an insoluble particle and an advancing solid/liquid interface. *Metall. Trans. A* **1992**, *23*, 669–680. [CrossRef]
22. Yu, T.; Deng, Q.L.; Dong, G.; Yang, J.G. Effects of Ta on microstructure and microhardness of Ni based laser clad coating. *Appl. Surf. Sci.* **2011**, *257*, 5098–5103. [CrossRef]
23. Du, B.S.; Zou, Z.D.; Wang, X.H.; Qu, S.Y. Laser cladding of in situ TiB_2/Fe composite coating on steel. *Appl. Surf. Sci.* **2008**, *254*, 6489–6494. [CrossRef]

Disclaimer/Publisher's Note: The statements, opinions and data contained in all publications are solely those of the individual author(s) and contributor(s) and not of MDPI and/or the editor(s). MDPI and/or the editor(s) disclaim responsibility for any injury to people or property resulting from any ideas, methods, instructions or products referred to in the content.